Chandra Discovery of a 100 kiloparsec X-Ray Jet in PKS 0637−752

Permanent link

Terms of Use

Share Your Story

CHANDRA DISCOVERY OF A 100 KILOPARSEC X-RAY JET IN PKS 0637−752

D. A. SCHWARTZ,[1] H. L. MARSHALL,[2] J. E. J. LOVELL,[3] B. G. PINER,[4] S. J. TINGAY,[3,4] M. BIRKINSHAW,[1,5] G. CHARTAS,[6]
M. ELVIS,[1] E. D. FEIGELSON,[6] K. K. GHOSH,[7] D. E. HARRIS,[1] H. HIRABAYASHI,[8] E. J. HOOPER,[1]
D. L. JAUNCEY,[3] K. M. LANZETTA,[9] S. MATHUR,[10] R. A. PRESTON,[4] W. H. TUCKER,[1]
S. VIRANI,[1] B. WILKES,[1] AND D. M. WORRALL[1,5]

ABSTRACT

The quasar PKS 0637−752, the first celestial X-ray target of the *Chandra X-Ray Observatory*, has revealed asymmetric X-ray structure extending from $3''$ to $12''$ west of the quasar, coincident with the inner portion of the jet previously detected in a 4.8 GHz radio image (Tingay et al. 1998). At a redshift of $z = 0.651$, the jet is the largest ($\gtrsim 100$ kpc in the plane of the sky) and most luminous ($\sim 10^{44.6}$ ergs s^{-1}) of the few so far detected in X-rays. This Letter presents a high-resolution X-ray image of the jet, from 42 ks of data when PKS 0637−752 was on-axis and ACIS-S was near the optimum focus. For the inner portion of the radio jet, the X-ray morphology closely matches that of new Australian Telescope Compact Array radio images at 4.8 and 8.6 GHz. Observations of the parsec-scale core using the very long baseline interferometry space observatory program mission show structure aligned with the X-ray jet, placing important constraints on the X-ray source models. *Hubble Space Telescope* images show that there are three small knots coincident with the peak radio and X-ray emission. Two of these are resolved, which we use to estimate the sizes of the X-ray and radio knots. The outer portion of the radio jet and a radio component to the east show no X-ray emission to a limit of about 100 times lower flux. The X-ray emission is difficult to explain with models that successfully account for extranuclear X-ray/radio structures in other active galaxies. We think the most plausible is a synchrotron self-Compton model, but this would imply extreme departures from the conventional minimum energy and/or homogeneity assumptions. We also rule out synchrotron or thermal bremsstrahlung models for the jet X-rays, unless multicomponent or ad hoc geometries are invoked.

Subject headings: quasars: individual (PKS 0637−752) — radio continuum: galaxies — X-rays: galaxies

1. INTRODUCTION

PKS 0637−752 was the first celestial X-ray target of the *Chandra X-ray Observatory* (Weisskopf et al. 2000). As a moderate strength point source it was used to locate the optical axis and focus of the X-ray mirror assembly. Surprisingly, even the first short, out-of-focus image clearly revealed an X-ray jet, coincident with the radio jet reported by Tingay et al. (1998). This Letter addresses the X-ray jet, which appears as a extension from $3''$ to $11''\!.5$ west of the quasar, with brighter condensations from $7''\!.5$ to $9''\!.5$. This corresponds[11] to an extension in the plane of the sky from ~ 30 to ~ 100 kpc from the nucleus, with an X-ray luminosity of $\sim 4.2 \times 10^{44}$ ergs s^{-1}: the largest and most luminous X-ray jet discovered to date. In a companion paper (Chartas et al. 2000) we examine the X-ray spectra of

the core and jet in more detail by adding substantial additional data where the detector was slightly out of focus.

PKS 0637−752 was identified with a pointlike object by Hunstead (1971), based on an accurate radio position, and a redshift of $z = 0.651$ was measured by Savage, Browne, & Bolton (1976). The *HEAO 1* all-sky survey suggested it as a 2–10 keV X-ray source (Wood et al. 1984). Definitive X-ray identification was made in the 0.3–3.5 keV band with the *Einstein Observatory* (Elvis & Fabbiano 1984), and numerous X-ray observations have since been made (see Yaqoob et al. 1998 and references therein); however, none approached the subarcsecond image quality of *Chandra* (Jerius et al. 2000) and so could not resolve the jet. The source is gamma-ray quiet (Fichtel et al. 1994), with a 2 σ upper limit of 4×10^{-8} photons cm^{-2} s^{-1} for gamma rays above 100 MeV.

Very long baseline interferometry (VLBI) space observatory program (VSOP) observations were rescheduled to overlap the *Chandra* observations to investigate links between the known parsec-scale jet (Tingay et al. 1998) and the X-ray emission from the quasar core. During the VSOP observations we also obtained Australian Telescope Compact Array (ATCA) radio images with comparable resolution to the *Chandra* images. We discuss the radio data in § 2.2. *Hubble Space Telescope* (*HST*) Wide Field Planetary Camera 2 (WFPC2) images were obtained fortuitously on 1999 May 30 and are discussed in § 2.3.

2. OBSERVATIONS

2.1. *X-Ray*

Six *Chandra* observations, totaling 42 ks when the target was on-axis and the detector was within 0.25 mm of focus,

[1] Harvard-Smithsonian Center for Astrophysics, 60 Garden Street, Cambridge, MA 02138; pks0637@head-cfa.harvard.edu.

[2] Massachusetts Institute of Technology, Center for Space Research, 70 Vassar Street, Cambridge, MA 02139.

[3] Australia Telescope National Facility/Commonwealth Scientific and Industrial Research Organisation, P.O. Box 76, Epping NSW 2121, Australia.

[4] Jet Propulsion Laboratory, California Institute of Technology, 4800 Oak Grove Drive, Pasadena, CA 91109.

[5] Department of Physics, University of Bristol, Tyndall Avenue, Bristol BS8 1TL, England, UK.

[6] Department of Astronomy and Astrophysics, Pennsylvania State University, 525 Davey Lab, University Park, PA 16802.

[7] NASA Marshall Space Flight Center, Huntsville, AL 35812.

[8] Institute of Space and Astronautical Science, 3-1-1 Yoshinodai, Sagamiharashi, Kanagawa 229, Japan.

[9] Department of Physics and Astronomy, State University of New York at Stony Brook, Stony Brook, NY 11794-3800.

[10] Department of Astronomy, Ohio State University, 140 West 18th Avenue, Columbus, OH 43210-1173.

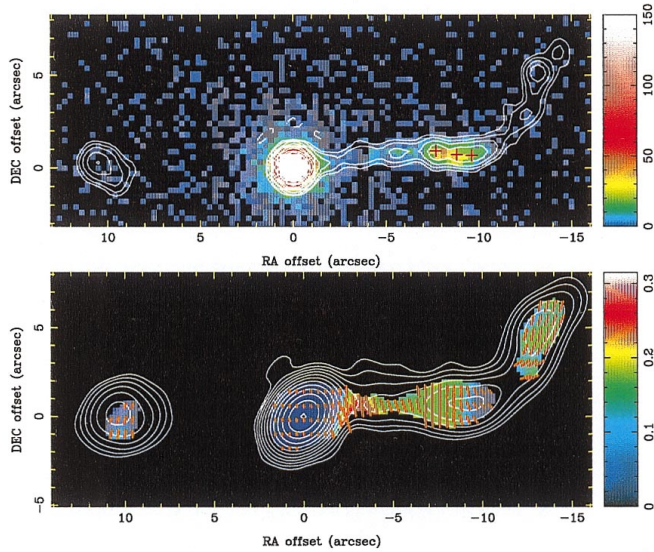[11] We use $H_0 = 50$ km s^{-1} Mpc^{-1} and $q_0 = 0$ throughout.

Fig. 1.—*Top*: Images of the quasar PKS 0637−752 in the X-ray (*false color*), the ATCA 8.6 GHz radio (*contours*), and optical (*plus signs*) bands. X-ray color scale is counts per $0\farcs3 \times 0\farcs3$ pixel. Radio contours are −1, 1, 2, 4, 8, 16, 32, 64, 128, 256, 512, 1024, and 2048 × 2.5 mJy beam^{-1}, where the restoring beam is circular with an FWHM of $0\farcs84$. *Bottom*: ATCA 4.8 GHz radio contours at 1, 2, 4, 8, 16, 32, 64, 128, 256, 512, 1024, and 2048 × 3 mJy beam^{-1}, the fractional polarization in false color; the direction of the electric vector is given by the red lines whose lengths are proportional to the fractional polarization. The bend in the radio jet, the change in radio polarization fraction and direction, and the termination of the X-ray emission are all coincident, $9\farcs5$–$11\farcs5$ west of the quasar.

were used to create an X-ray image. We use the full energy band of the back side–illuminated S3 CCD chip, ∼0.3–10 keV.

The point-spread function (PSF) of the resultant core image has a half-power radius of $0\farcs42$ and a 90% encircled energy radius of $1\farcs55$. The image quality of the quasar core is broadened slightly by event pileup, indicated by overrepresentation of the high grades as well as the high counting rates of ∼0.4 s^{-1}. In the direction perpendicular to the jet, the core fits a Gaussian profile with an rms of $0\farcs37$. The jet is faint enough that pileup is not significant at any point.

The X-ray and radio images are shown in Figure 1. The X-ray jet, which corresponds to the inner portion of the western radio jet before the bend to the northwest, separates into two regions: within 7″ of the core the X-ray flux is somewhat faint and maintains a position angle (P.A.) of −82°; at about 7″ from the core the jet bends distinctly to the south to a P.A. of −86°, and the flux is about 3 times greater. The increased brightening may be dominated by three pointlike knots, as detected with *HST* and shown as the plus signs. In the brighter parts of the jet, a fit to the cross-jet profile is consistent with the core PSF; thus, the jet is unresolved in this direction, with an intrinsic width less than $0\farcs3$ FWHM.

We detect a net 1205 X-ray counts from the entire inner, western jet, defined as a rectangle from 3″ to $11\farcs5$ west and from $0\farcs5$ south to 2″ north of the quasar. For the power-law energy index[12] of $\alpha = 0.85 \pm 0.08$ (Chartas et al. 2000), this corresponds to a measured 2–10 keV flux of 1.2×10^{-13} ergs cm^{-2} s^{-1}, or a spectral normalization at 1 keV of 5.9×10^{-14} ergs cm^{-2} s^{-1} keV^{-1}. That is, the flux density is 25 nJy at 2.4×10^{17} Hz. We fixed the Galactic absorption at $N_H = 9 \times 10^{20}$ cm^{-2}.

Figure 2 plots the X-ray and radio surface brightness as a

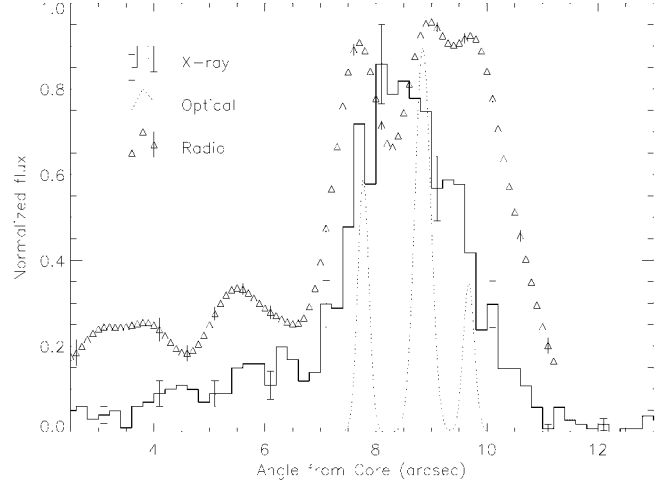Fig. 2.—Radio and X-ray profiles of the large-scale jet in PKS 0637−752. The X-ray histogram gives counts in a $0\farcs2$ bin, normalized to unity at 69 counts s^{-1} bin^{-1}. The triangles are 8.6 GHz flux density per beam, normalized to unity at 0.04 Jy. The dashed Gaussian curves mark the positions of knots detected in the *HST* optical images, but we do not actually measure the profiles. The total flux for these three knots is 0.2, 0.28, and 0.094 μJy, respectively, east to west.

function of the distance west of the quasar core, integrated ± 1″ perpendicular to the jet. There are three distinct, partially resolved radio peaks or knots in the brighter part of the inner western jet, which we designate by their direction and distance from the core using the notation WK7.8, WK8.9, and WK9.7. The enhanced X-ray emission is closely associated with those knots but not in exact detail. In particular, the X-ray flux falls off more steeply past $9\farcs5$. The ratio of the flux densities at 1 keV to 8.6 GHz varies by no more than a factor of 2 from the value 1.3×10^{-7} in the region ∼4″–$9\farcs5$ west of the quasar core.

2.2. *Radio*

PKS 0637−752 is the subject of ongoing VSOP (Hirabayashi et al. 1998) observations to monitor its parsec-scale evolution (Tingay et al. 2000), with one of the VSOP observations being rescheduled to overlap the first *Chandra* observation. ATCA observations were scheduled in parallel with the VSOP observations to provide 1″ and 2″ resolution radio images at 8.6 and 4.8 GHz, respectively, to complement the *Chandra* images.

These ATCA images confirmed the remarkable coincidence of the radio and X-ray jets. Subsequent observations were made to improve image sensitivity and to determine the jet polarization. The inner west radio jet is optically thin with a spectral index of 0.81, and the polarization is 10%–20%. The *E*-vectors are perpendicular to the jet where X-rays are detected, but as the X-ray flux decreases near the bend in the radio jet, the polarization P.A. begins to change so that the *E*-vectors become parallel to the jet's center line for the remainder of the radio jet.

We have reanalyzed our VLBI observations (Lovell et al. 2000; Chartas et al. 2000) to search for the presence of more compact components within the radio knots. We find that the knots are indeed resolved at $0\farcs05$ resolution with no more than 5 mJy, about 14% remaining at this resolution. This suggests that the radio knots are most likely low surface brightness "hot spots."

A rotation measure image was constructed from the polar-

---

[12] We use $f_\nu \propto \nu^{-\alpha}$.

ization data at the two frequencies. Faraday rotation was detected in the quasar core ($RM = 80$ rad m^{-2}) but *not* in the jet, with an upper limit of ± 30 rad m^{-2}. The absence of significant Faraday rotation implies that the intrinsic magnetic field in the jet is perpendicular to the observed E-vectors in Figure 2. That is, the magnetic field is longitudinal where the X-ray emission is strong and perpendicular to the jet where we do not detect X-ray emission.

The VSOP observations show that PKS 0637−752 displays apparent superluminal motion in its parsec-scale jet, co-aligned with the inner portion of the arcsecond-scale radio jet (Lovell et al. 2000). Six data sets covering 1995–1999 (four from the US Naval Observatory's geodetic VLBI database [Piner & Kingham 1998], two from VSOP) allow the motion of three parsec-scale features to be measured. Linear least-squares fits to the separation of these features from the VLBI core versus time yield proper motions of 0.41 ± 0.03, 0.29 ± 0.05, and 0.36 ± 0.09 mas yr^{-1} from the outermost component inward (Lovell et al. 2000). These proper motions and associated errors are just consistent with all three components moving at the weighted average proper motion of 0.36 ± 0.02 mas yr^{-1}, which corresponds to an apparent speed of $17.8c \pm 1.0c$. Since the apparent transverse speed is given by $\beta_{\rm obs} = \beta \sin \theta/(1 - \beta \cos \theta)$ (Rees 1966), this apparent speed places limits on the bulk Lorentz factor in the VLBI jet and the angle of the VLBI jet to the line of sight of $\Gamma > 17.8$ and $\theta < 6°.4$, respectively. Since the parsec-scale and arcsecond-scale radio jets are very well aligned, unless the jet goes through a large bend in a plane perpendicular to the plane of sky the actual length of the X-ray jet would be at least 940 kpc.

2.3. *Optical*

An optical image of PKS 0637−752 was obtained with the *HST* WFPC2 using the F702W filter. Three observations were combined in order to eliminate cosmic rays, giving a total exposure time of 2100 s. Three distinct knots are detected within the radio image contours 7″.7, 8″.8, and 9″.6 west of the core (Fig. 1). These have fluxes 0.2, 0.28, and 0.094 μJy, respectively, at an effective frequency 4.3×10^{14} Hz (6969 Å). We have assumed an energy spectrum $f_\nu \propto \nu^{-1}$ to deduce the flux densities and effective frequency. The knot at 7″.7 is not resolved, while the other two are about 0″.3 in diameter.

The quasar image is saturated, so it is difficult to detect sources within about 2″ of the quasar core. We estimate that the knots can be located relative to the quasar to an accuracy of about 0″.07. The *HST* image also shows the presence of a group of faint galaxies, ∼100 kpc in radius, surrounding the quasar.

3. DISCUSSION

We will discuss the X-ray emission specifically from the knots 7″.8 and 8″.9 west of the nucleus, which contain most of the luminosity of the inner western jet and which are coincident with radio knots and the optical emission detected by *HST*. We consider in turn synchrotron, thermal bremsstrahlung, and inverse Compton for the X-ray emission mechanism.

3.1. *Synchrotron*

The strong polarization shows that the radio emission arises from synchrotron radiation. Standard models assume a power-law population of relativistic electrons with a density $n(\gamma) = n_0 \gamma^{-m}$, where γ is the Lorentz factor. The radio spectral index $\alpha = (m - 1)/2$ is observed to be 0.81, so that $m =$

2.62. A natural hypothesis is that the X-rays are also synchrotron radiation from the same population of electrons. However, the optical flux falls a factor of 10 below such a continuous spectrum and therefore rules out such a simple model. The absence of optical emission at the level of 5.6 μJy, which would be required, implies that the high-energy cutoff to the electron spectrum be such as to cause the radio spectrum to steepen at $\nu < 3 \times 10^{12}$ Hz. For the X-rays to result from synchrotron emission there would have to be an independent population of electrons with a similar index $m = 2.7$ in the energy region emitting the X-rays but that flattened at lower γ to avoid overproducing the optical. There then would be no apparent reason for the existing spatial correlation of the radio and X-ray emission.

3.2. *Thermal Bremsstrahlung*

Although the data allow a fit to a thermal spectrum providing kT is at least 4 keV (Chartas et al. 2000), thermal bremsstrahlung is not a viable origin for the X-ray emission unless a contrived geometry is invoked. Taking an upper limit size of 0″.4 for the diameter of a cylindrical jet, it would require an electron density of $n_e = 2$ cm^{-3} to produce the measured luminosity. But the upper limit to the rotation measure places a limit $n_e < 3.7 \times 10^{-5}/(HL)$. Even if the magnetic field were as low as 1 μG, a path length of only $L = 20$ pc through such a thermal plasma would exceed the rotation measure limit.

3.3. *Inverse Compton*

3.3.1. *Synchrotron Self-Compton*

The obvious remaining mechanism is inverse Compton, which can successfully explain the *Chandra* observations of hot spots in 3C 295 (Harris et al. 2000). Because we have measured the X-ray spectral index to be nearly the same as the 4.8–8.6 GHz radio index, it is natural to assume that both arise from the same population of relativistic electrons. In inverse Compton scattering scenarios the synchrotron radio emission is typically produced by the higher energy electrons while the X-rays are produced by lower energy electrons. It is then natural to have high-energy and low-energy cutoffs such that the optical emission is no larger than observed. In particular, we expect electrons of $\gamma \sim 10^4$ to scatter radio seed photons at ∼10 GHz up to the *Chandra* X-ray energy range. The second-order scattering would already be limited by the Klein-Nishina cross section, and we would have no "Compton Catastrophe."

To estimate the expected X-ray flux, we first apply standard synchrotron theory (e.g., Miley 1980) to estimate the magnetic field H and particle density n_0, giving a minimum total energy. For example, if WK7.8 is a sphere of 0″.3 diameter, uniformly filled with magnetic field and electrons and with no proton component, then $H \simeq 320$ μG and the total minimum energy in that sphere is $U_{\rm min} \simeq 1.5 \times 10^{57}$ ergs. We have assumed the radio spectrum extends from 10 MHz up to 500 GHz. In this situation, the predicted X-ray flux is ∼300 times less than observed. Such a model would satisfactorily explain the lack of X-ray emission beyond the point where the radio jet bends toward the northwest.

The radio synchrotron photons would have an energy density 8×10^{-11} ergs cm^{-3} in the knot if we assume the radio spectrum extends up to 500 GHz. By comparison, the minimum energy magnetic field calculated above would have an energy density $H^2/(8\pi) = 3.8 \times 10^{-9}$ ergs cm^{-3}. In order that there be 300 times more relativistic electrons, and to predict the same GHz radio flux, we must assume the magnetic field is ∼6 μG.

To balance the radio–to–X-ray flux ratios from the entire inner western jet to within a factor of 2 as is observed then requires the apparently smooth jet to be composed primarily of many radio knots, with the particle and field densities delicately balanced to produce the X-rays. Such a gross departure from equipartition, increasing the total energy by a factor of ∼1000, would pose significant problems for models of the particle acceleration and the jet confinement.

We can make any inverse Compton scenario more realistic by assuming that the magnetic field strength need not be constant throughout the volume. The exact distribution of field strength with volume would be nonunique. We must assume that the relativistic particles throughout the entire volume produce the X-rays, while a small fraction of the jet containing high magnetic fields provides essentially all of the radio emission. Such inhomogeneity and/or departure from equiparition may be plausible when we note the bend in the radio jet, the dramatic change in radio polarization, and the decrease in the X-ray flux, all coincident in the region $9''.5–11''.5$ west of the nucleus. These may be indicative of shock activity causing particle acceleration.

3.3.2. *Alternative Photon Sources*

Alternate inverse Compton models could use some source of unseen photons. The equivalent luminosity of these photons in WK7.8 would have to be 4×10^{45} ergs s^{-1}. If the core is the source of this luminosity, it must radiate at an unreasonable value of 2×10^{49} ergs s^{-1}, considering that the knot subtends a solid angle of only 1.9×10^{-4} sr. We cannot rule out that a Doppler-boosted beam is shining on the knots but out of our direct line of sight (Perez-Fournon 1985). This beam would presumably be optical/IR emission. However, if this could happen then when we *did* fall in such a beam we would infer optical luminosities of $\gtrsim 10^{49}$ ergs s^{-1} for such a source. Such objects are not observed.

3.3.3. *Relativistic Beaming*

We might invoke relativistic beaming of the jet and knots to reconcile the observed X-ray flux with the apparent equipartition magnetic field. The conventional formula (Jones, O'Dell, & Stein 1974) for the ratio of synchrotron self-Compton (SSC) X-ray–to–radio flux is multiplied by a factor $\delta^{-4-2\alpha}$ where $\delta = 1/[\Gamma(1 - \beta \cos \theta)]$ is the beaming factor of matter moving with bulk Lorentz factor Γ at an angle θ to the line of sight (see Madejski & Schwartz 1983). We can explain the absence of X-rays from a putative eastern jet by Doppler

suppression if $\Gamma = 8$, and then a value $\delta = 0.3$ would reconcile a minimum energy radio source with the observed X-rays being produced by SSC. This would require the X-ray jet to be at an angle of 53° to our line of sight. Since the VLBI jet must be at an angle less than about 6°, and since the VLBI jet and 100 kpc jet *appear* to be in the same direction, the required bending would have to occur about an axis that is very nearly in the plane of the sky, an unlikely coincidence. Even with such a coincidence, we note that the apparent radio luminosity of 3×10^{43} ergs s^{-1} would actually be a factor $\delta^{-(2+\alpha)} = 25$ higher in the rest frame, and for similar sources beamed toward us we would infer a radio luminosity of 2×10^{46} ergs s^{-1}. This exceeds observed blazar radio luminosities.

4. CONCLUSIONS

Discovery of the largest and most luminous X-ray jet in the very first celestial X-ray target of *Chandra* has dramatically proven the power of this observatory. It immediately shows the value of the *two-dimensional* angular resolution improvement of a factor of 100 over the best previous missions. It is likely that many further X-ray jets will be detected in extragalactic radio sources. The X-rays place difficult constraints on the physical conditions, eliminating standard scenarios, and will surely have important astrophysical consequences, e.g., in terms of understanding regions of particle acceleration, inhomogeneities of magnetic field structures, and/or extreme departures from equipartition conditions. While it seems that inverse Compton emission from the same electrons producing the synchrotron radio emission is the most plausible source of the
X-ray emission, we have noted difficulties with the specific scenarios we have considered.

REFERENCES

Chartas, G., et al. 2000, ApJ, in press
Elvis, M., & Fabbiano, G. 1984, ApJ, 280, 91
Fichtel, C. E., et al. 1994, ApJS, 94, 551
Harris, D. E., et al. 2000, ApJ, 530, L81
Hirabayashi, H., et al. 1998, Science, 281, 1825
Hunstead, R. W. 1971, MNRAS, 152, 277
Jerius, D., Edgar, R. J., Gaetz, T. J., McNamara, B. R., Schwartz, D. A., VanSpeybroeck, L. P., & Zhao, P. 2000, Proc. SPIE, in press
Jones, T. W., O'Dell, S. L., & Stein, W. A. 1974, ApJ, 188, 353
Lovell, J. E. J., et al. 2000, in Astrophysical Phenomena Revealed by Space VLBI, ed. H. Hirabayashi, P. G. Edwards, & D. W. Murphy (Sagamihara: ISAS), 215
Madejski, G. M., & Schwartz, D. A. 1983, ApJ, 275, 467

Miley, G. 1980, ARA&A, 18, 165
Perez-Fournon, I. 1985, in Active Galactic Nuclei, ed. J. E. Dyson (Manchester: Manchester Univ. Press), 300
Piner, B. G., & Kingham, K. A. 1998, ApJ, 507, 706
Rees, M. J. 1966, Nature, 211, 468
Savage, A., Browne, I. W. A., & Bolton, J. G. 1976, MNRAS, 177, 77P
Tingay, S. J., et al. 1998, ApJ, 497, 594
———. 2000, Adv. Space Res., 26, 677
Weisskopf, M. C., Tananbaum, H. D., Van Speybroeck, L. P., & O'Dell, S. L. 2000, Proc. SPIE, in press
Wood, K. S., et al. 1984, ApJS, 56, 507
Yaqoob, T., George, I. M., Turner, T. J., Nandra, K., Ptak, A., & Serlemitsos, P. J. 1998, ApJ, 505, L87